Exchange Fields and Optical Zeeman Effect in $ErFeO_3$

D. L. Wood, L. M. Holmes, and J. P. Remeika
Bell Telephone Laboratories, Murray Hill, New Jersey 07974
(Received 23 April 1969)

The optical spectra of $ErFeO_3$ with and without an external magnetic field along each of the three principal crystal axes are reported. The exchange splitting of Er^{3+} levels in zero applied field and the additional splittings due to the external field, at 77°K, are analyzed in terms of a two-sublattice model for the Er^{3+} ions. Values are derived for the g-tensor components and site-axis directions for the two lowest levels of Er^{3+} at $E=0$ and $E=45.7$ cm^{-1}. Interactions with the Fe^{3+} spins are included by means of an effective field $H_{eff}=12$ kOe at the Er^{3+} sites. The parameters derived from the optical spectra are used to calculate the sublattice magnetizations for Er^{3+}. Assuming a contribution from the Fe^{3+} spins similar to that in $YFeO_3$, a compensation point is predicted near the observed temperature $T_0\approx45$°K. The magnetic dipolar contribution to H_{eff} is shown to be small, and the exchange contribution lies nearly along the b axis. Above the spin-reorientation temperature $T>T_r$, the Fe^{3+}-Er^{3+} exchange splitting becomes smaller than the optical linewidth. The optical data give $H_{eff}(T<T_r)/H_{eff}\ (T>T_r)>4$, and this result is shown to be consistent with the value for $H_{eff}\ (T>T_r)$ obtained by other methods. It is suggested that either a model with more than two sublattices for the Fe^{3+} spins must apply for $ErFeO_3$, or there must be significant antisymmetric exchange coupling between the Er^{3+} and Fe^{3+} ions.

INTRODUCTION

It is well known that the rare-earth orthoferrites are optically transparent in the near infrared and in thin sections on into the visible.[1–8] This transparent region permits the study of many rare-earth internal transitions, which take the form of sharp lines in absorption. In $ErFeO_3$ the optical linewidth is narrow enough to observe the exchange splitting of the rare-earth levels due to the coupling with the iron ions in the structure.[5,8] The zero-field exchange splitting for Er^{3+} has been measured for the lowest level from the optical spectrum, and the ordering of the rare earth near 4.2°K has been observed this way.[5] We have observed[8] that the exchange splitting of the Er^{3+} levels can no longer be observed above the spin-reorientation temperature T_r, and we have analyzed the additional splittings produced by an external magnetic field applied in various directions. We report here these characteristics of the spectra having to do with the magnetic properties of $ErFeO_3$, and, in addition, we give new data on the energy levels of Er^{3+} in this crystal structure.

CRYSTAL STRUCTURE AND MAGNETIC PROPERTIES

The crystal structure of the weak ferromagnet $ErFeO_3$ is orthorhombic (space group $Pbnm$)[9,10] with four formula units in a unit cell. The magnetic structure has been studied by neutron-diffraction techniques.[11] It was found that the Fe^{3+} spins may be described by a "G-type" antiferromagnetic arrangement in which each Fe^{3+} spin is surrounded by six antiparallel neighbors. The spins are canted relative to one another, resulting in a spontaneous magnetization, but the canting angle is very small and was not detected in the neutron-diffraction study. By comparing bulk magnetization and Mössbauer absorption data, a canting angle equal to 8 mrad was determined[12] for $ErFeO_3$.

Below the Curie temperature[13] of $ErFeO_3$, $T_c=636$°K, the spontaneous magnetization initially builds up along the c axis of the crystal. From the neutron-diffraction study,[11] the antiferromagnetic Fe^{3+} sublattices are polarized along the $\pm a$ axes. They must, of course, be canted slightly towards c to give the observed spontaneous magnetization. The most probable magnetic symmetry may be described, following Bertaut,[14] by the symbols $G_xA_yF_z$, where G_x refers to the basic antiferromagnetic arrangement of the Fe^{3+} sublattices along the $\pm a$ axes, A_y refers to possible canting of the sublattices towards the $\pm b$ axes, and F_z refers to the canting towards the c axis which results in a spontaneous magnetization. The various Fe^{3+} spin symmetries are pictured clearly in a recent review article by White.[15] The canting associated with the symbol A_y may be referred to as "antiferromagnetic" in the sense that the different sublattices are canted in opposite directions, resulting in no net contribution to the spontaneous magnetization. Although the A_y components are allowed

[1] K. A. Wickersheim and R. A. Lefever, J. Chem. Phys. **36**, 844 (1962).
[2] D. L. Wood and J. P. Remeika, J. Appl. Phys. **38**, 1038 (1967).
[3] E. D. Kolb, D. L. Wood, and R. A. Laudise, J. Appl. Phys. **39**, 1362 (1968).
[4] E. M. Gyorgy, J. P. Remeika, and D. L. Wood, J. Appl. Phys. **39**, 3499 (1968).
[5] R. Faulhaber, S. Hüfner, E. Orlich, and H. Schuchert, Z. Physik **204**, 101 (1967).
[6] R. C. Sherwood, J. P. Remeika, and H. J. Williams, J. Appl. Phys. **30**, 217 (1959).
[7] C. A. Fowler, Jr., E. M. Fryer, B. L. Brandt, and R. A. Isaacson, J. Appl. Phys. **34**, 2064 (1963).
[8] D. L. Wood, J. P. Remeika, L. M. Holmes, and E. M. Gyorgy, J. Appl. Phys. **40**, 1245 (1969).
[9] S. Geller and E. A. Wood, Acta Cryst. **9**, 563 (1956).
[10] M. Eibschütz, Acta Cryst. **19**, 337 (1965).
[11] W. C. Koehler, E. O. Wollan, and M. K. Wilkinson, Phys. Rev. **118**, 58 (1960).
[12] D. Treves, J. Appl. Phys. **36**, 1033 (1965).
[13] M. Eibschütz, S. Shtrikman, and D. Treves, Phys. Rev. **156**, 562 (1967).
[14] E. F. Bertaut, in *Magnetism*, edited by G. T. Rado and H. Suhl (Academic Press Inc., New York, 1963), Vol. III, p. 149.
[15] R. L. White, J. Appl. Phys. **40**, 1061 (1969).

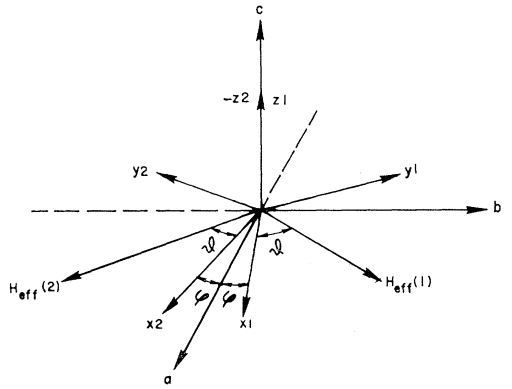

FIG. 1. Principal magnetic axes (x_i,y_i,z_i) for two inequivalent Er^{3+} sites in $ErFeO_3$, and effective fields (H_{eff}) below the spin reorientation temperature $(T<T_r=102°K)$.

by symmetry, they have not been observed experimentally in any of the rare-earth orthoferrites.

The spontaneous magnetization remains along the c axis until the temperature approaches $T_r=102°K$. In an interval of temperature equaling about 10°K and centered on T_r, the spontaneous magnetization rotates from the c axis to the a axis of the crystal.[6,8] This spin reorientation may be pictured[15] in terms of a rotation of the (nearly) antiferromagnetic Fe^{3+} sublattices from the $\pm a$ axes to the $\pm c$ axes (i.e., a change from G_x symmetry to G_z symmetry). The rotation of the G component for the Fe^{3+} spins has been followed[16] by neutron diffraction in $TmFeO_3$, which undergoes a similar transition. For $T<T_r$, the magnetic symmetry may be described by the symbols[14] $F_xC_yG_z$, where F_x refers to the canting of the sublattices towards the a axis, and C_y refers to another "antiferromagnetic" canting of the sublattices towards the $\pm b$ axes. As with the A_y components at $T>T_r$, the C_y components at $T<T_r$ have not been detected in $ErFeO_3$. The A_y and C_y components are undoubtably small, and they are sometimes neglected, leading effectively to a reduction in the number of Fe^{3+} sublattices from four to two.

At liquid-helium temperatures, the rare-earth–rare-earth interactions become important, and a third magnetic structure develops.[11] We shall not describe that, since the measurements reported here for the Er^{3+} absorption spectrum were recorded for sample temperatures above 5°K.

The rare-earth ions in $ErFeO_3$ are on sites of monoclinic point symmetry C_s.[9] Two magnetically inequivalent sites are present, as illustrated in Fig. 1. Interactions with the Fe^{3+} spins may be treated in terms of effective fields H_{eff} at the Er^{3+} sites. Symmetry considerations indicate that the effective fields at the two sites are symmetrically disposed relative to the local magnetic axes. For $T>T_r$, H_{eff} is along the local z axis, whereas for $T<T_r$, H_{eff} is in the local x-y plane (Fig. 1). Ions on the two sites are therefore equivalent in the absence of external fields.

The crystals used in this work were prepared by slow cooling of a mixture of the appropriate oxides in a flux of PbO and B_2O_3.[17]

TABLE I. Energy levels of Er^{3+} in $ErFeO_3$.

	E (cm^{-1})	δ (cm^{-1})	g_z		E (cm^{-1})	δ (cm^{-1})	g_z
$^4I_{15/2}$	0	3.3	5.76	$^4I_{11/2}$	10 221.0	1.0	3.0
	45.7	4.4	1.78		10 249.4	0.7	3.4
	109.2	0	1.0		10 261.7	2.3	···
	131.3	2.5	2.5		10 280.5	0.2	0.9
	166	6.0	···		10 301.7	1.0	0
	247	···	···		10 355.0	1.8	···
	279	···	···				
	411	···	···	$^4I_{9/2}$	12 379.5	0.8	2.5
					12 423.1	···	0
$^4I_{13/2}$	6551.3				12 510.5	0.4	1.6
	6587.5				12 562.8	0.6	···
	6620.7				12 608.7	···	1.2
	6641.8						
	6701.5			$^4F_{9/2}$	15 190.2	2.4	0
	6718.6				15 225.0	0.4	1.3
	6818.5				15 298.6	0.2	2.6
					15 334.9	1.1	4.2
					15 392.5	0.2	0

OPTICAL SPECTRUM

An over-all view of the spectrum of $ErFeO_3$ is given in Fig. 2, where $\alpha=(1/t)\log_{10}I_0/I$ (t is the thickness, and I_0 and I are the incident and transmitted intensities) is plotted against wavelength. The transparent region reaches from about 1.3 to 8 μ, and the first two crystal field bands of the Fe^{3+} ion show at 1 and 0.7 μ. The groups of sharp lines belong to the Er^{3+} ion, and the transitions involved are identified in the figure.

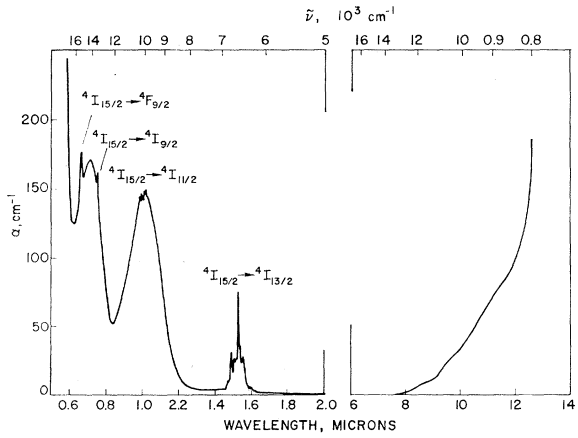

FIG. 2. Spectrum of $ErFeO_3$ at low resolution showing the "transparent" window from 1.3 to 8 μ, the sharp line rare-earth transitions, the first two Fe^{3+} crystal field bands (0.7 and 1.0 μ), and the lattice vibration absorption region beyond 8 μ. Here $\alpha=(1/t)\log_{10}I_0/I$.

[16] J. A. Leake, G. Shirane, and J. P. Remeika, Solid State Commun. 6, 15 (1968).

[17] J. P. Remeika and T. Y. Kometani, Mater. Res. Bull. 3, 895 (1968).

In the transparent region the apparent absorption coefficient for the background is dependent on the quality of the crystals, and the best we have measured was $\alpha = 0.6$ cm^{-1}, some 20× larger than for the best iron garnet.[18] Even in the strongly absorbing region below 1.3 μ, however, it is possible to have adequate transmission for good absorption measurements in thin sections, and Fig. 3 shows in more detail the four sharp line groups identified in Fig. 2. For each line group there are, as expected, $\frac{1}{2}(2J+1)$ crystal field lines at low temperatures as a result of transitions between levels produced by the electrostatic perturbation of the free-ion term by the ligand charge. The location of the upper states is uniquely determined from absorption spectra at low temperatures, but the location of the levels in the ground manifold is not so direct. These extend over a range of about 400 cm^{-1}, and appreciable population of the lower members at temperatures below room temperature occurs. Thus the locations of these lower members have been determined from measurements of absorption intensity versus temperature, and from the frequency differences between the lines disappearing at low temperatures and those which did not. In our analysis of these data we plotted peak intensity versus temperature for each line showing a variation, and compared the curve with that calculated for the entire energy-level scheme using initially the frequency difference data alone. It was required that these two methods agree before the location of a level was accepted. As a final check, the fluorescence spectrum at low temperatures yields a plot of the ground manifold levels. We found that the pure $ErFeO_3$ did not fluoresce, but diluted samples containing about 10% Er in $GdFeO_3$ did show fluorescence near 1.6 μ at 4.2°K. The difference between the absorption spectrum of the diluted Er in $GdFeO_3$ and that of $ErFeO_3$ was very little, so we believe that the level locations from fluorescence are the same as those from the absorption spectrum. The results of these analyses of the observed spectra are tabulated as energy-level locations in the first column of Table I.

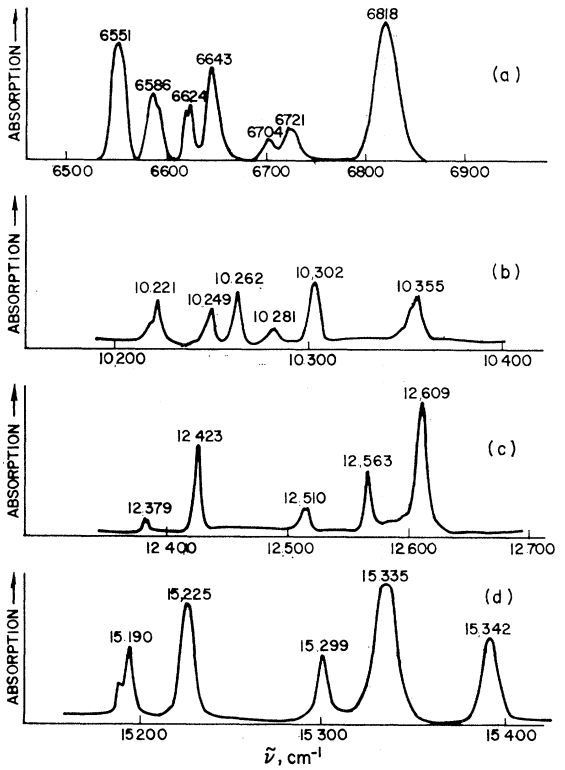

FIG. 3. Details of the sharp absorption lines due to Er^{3+} in $ErFeO_3$ at 5°K. Curves are taken from microphotometer traces of photographic records except for (a) which was measured with a scanning monochromator and photoconducting detector.

[18] R. C. LeCraw, D. L. Wood, J. F. Dillon, Jr., and J. P. Remeika, Appl. Phys. Letters 7, 27 (1965).

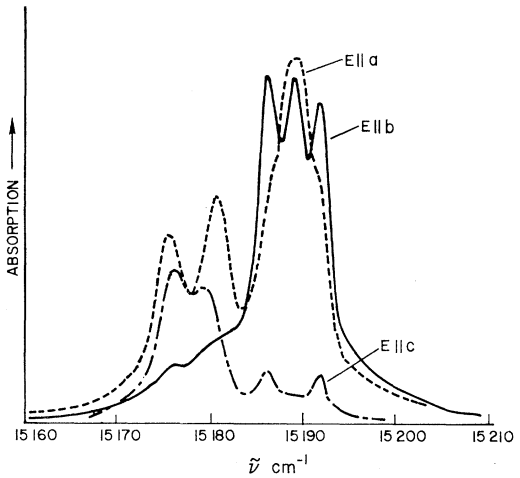

FIG. 4. Details of the exchange splitting and pleochroism (trichroism) of two lines in the spectrum of $ErFeO_3$. The patterns for each line arise from transitions between components of two Kramers doublets split by the Fe-Er exchange field. Full line, absorption with **E** vector of incident radiation parallel to the crystal b axis, dashed line $\mathbf{E}\|a$, and dot-dash line $\mathbf{E}\|c$.

DICHROISM AND EXCHANGE SPLITTING

The symmetry of the site for the rare earth is low,[9] having only a mirror plane (C_s), so the crystal field removes all but the Kramers degeneracy of the Er^{3+} ion levels. No true selection rules are expected for an ion on a C_s site, but large dichroic ratios are permitted, and they are actually observed, giving qualitatively different spectra for radiation polarized along the three principal axes. In addition, each Kramers doublet level may split in the exchange field due to the iron ions, and various Zeeman-like patterns are expected, depending on the relative magnitudes of the upper- and lower-state splittings. Figure 4 shows these features for two transitions in the group of lines near 6500 Å. The transition near 15190 cm^{-1} shows three components with a very large intensity for $\mathbf{E}\|a$ or b, but with a very small intensity for $\mathbf{E}\|c$. The transition near 15178 cm^{-1} shows a four-line pattern with weak intensity for $\mathbf{E}\|b$. Among

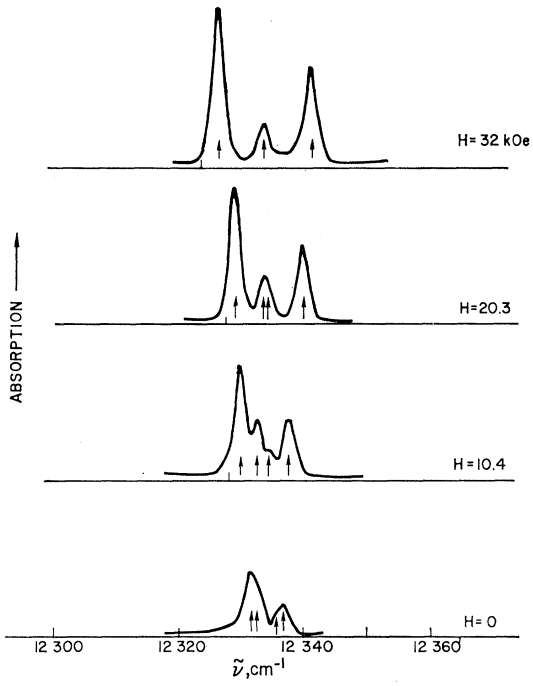

FIG. 5. Details of the Zeeman effect for a single line of Er^{3+} in $ErFeO_3$ for $\mathbf{H}\|c$ and $\mathbf{E}\|c$. Four components are detectable at $H=0$ with upper- and lower-state splittings of 0.8 and 4.4 cm^{-1}, respectively. At $H=32$ kOe, both states are split by 7.6 cm^{-1}, giving a three-line pattern.

the 39 transitions observed with enough resolution to measure the zero-field exchange splitting, examples of one-, two-, three-, and four-line patterns were recorded, and these were interpreted in terms of transitions between pairs of levels to derive the actual level splittings.

Because the linewidth is an appreciable fraction of the exchange splitting, the fine structure in the line patterns was often partially obscured, and it was necessary to fit the zero-field patterns simultaneously for related groups of lines. This procedure is based on the requirement that the splitting of a given level must be the same for every transition ending or originating on that level. By fitting the patterns first independently, and then adjusting the fitting to be consistent for all the related lines taking their width into consideration, we arrived at the zero-field splittings δ, shown in the second column of Table I.

ZEEMAN PATTERNS FOR $H\|c$ AT 77°K

When an external field is applied to the crystal additional level splittings occur and the nature of the splittings depends very much on the direction in which the field is applied. For H parallel to the a or c axis, the patterns are relatively simple one-, two-, three, or four-line patterns. For H parallel to the b axis, the patterns are more complicated, sometimes involving as many as eight components. Consider first the case of the magnetic field along the crystal c axis. The four Er^{3+} sites in each unit cell all have their local z axes parallel to the crystal c axis, and the exchange field lies in the a-b plane. The latter is not appreciably rotated by moderate external fields such as were applied here ($H<32$ kOe). Thus the levels start with the exchange splitting, and simply split further with increasing external field. An example of this is shown in Fig. 5, where the spectrum for a sample at 77°K shows four components barely discernable in the zero-field pattern, indicating a different upper- and lower-state splitting. As the field is increased the four components become more clearly resolved, and then merge into the three-line pattern characteristic of equal upper- and lower-state splittings. Obviously, the g factor for the state with the smaller zero-field splitting is greater than that of the other. By analyzing such patterns as these the g factors for H parallel to the site z axis can be determined from the nonlinear relation given as the first entry in Table II. There $2W(c)$ is the energy separation of the level components, $2\beta\delta$ is the zero-field separation of the level components, H is the external field strength, $\beta=4.67\times10^{-5}$ cm^{-1}/Oe, and H_{eff} is the effective field. It is relatively straightforward in this case to go from the observed frequencies to the level splittings, and hence to the appropriate g factor via the nonlinear Zeeman expression indicated. The results are given in the third column of Table I for each level whose patterns could be analyzed.

ZEEMAN PATTERNS FOR $H\|a$ OR b AT 77°K

When H is applied along the a or b axes, the situation is more complicated, and the observed Zeeman patterns are more difficult to interpret. On the other hand, the successful analysis of the patterns yields important information about the exchange field at the rare-earth ions, and on the site orientation as well. In order to explain the situation, we discuss next the model we have used for the interpretation.

In each rare-earth site the exact orientations of the x and y axes are not restricted by symmetry to lie in any particular direction, although they are constrained to lie in the a-b plane. Similarly, the effective field representing the exchange between the rare-earth and the

TABLE II. Formulas for Er^{3+} level splittings in $ErFeO_3$ at $T=77$°K.

Crystal axis	Splitting
$\mathbf{H}\|c$	$W(c)=\pm\beta(\delta^2+g_z^2H^2)^{1/2}$, where $\delta=(g_x^2\cos^2\vartheta+g_y^2\sin^2\vartheta)^{1/2}H_{\text{eff}}$
$\mathbf{H}\|a$	$W(a)=\pm\beta[g_x^2(H_{\text{eff}}\cos\vartheta+H\cos\varphi)^2+g_y^2(H_{\text{eff}}\sin\vartheta-H\sin\varphi)^2]^{1/2}$
$\mathbf{H}\|b$	$W(1b)=\pm\beta[g_x^2(H_{\text{eff}}\cos\vartheta+H\sin\varphi)^2+g_y^2(H_{\text{eff}}\sin\vartheta+H\cos\varphi)^2]^{1/2}$, $W(2b)=\pm\beta[g_x^2(H_{\text{eff}}\cos\vartheta-H\sin\varphi)^2+g_y^2(H_{\text{eff}}\sin\vartheta-H\cos\varphi)^2]^{1/2}$

iron ions also is constrained to lie in the a-b plane, but the direction in the plane is not fixed by symmetry. Thus the situation can be represented as shown in Fig. 1. The angle between the site x axis and the crystal a axis is φ, and the angle between the site x axis and the effective field is ϑ, but by symmetry ϑ and φ are the same for both sites. Then the energy splitting for H applied along a is given by the nonlinear expression for $W(a)$ given as the second entry in Table II. The symbols are identified as before. It is noteworthy that it is possible for the zero-field splitting to collapse as the external field is increased. However, there would still be a single set of levels, since both sites have the same splitting due to the presence of the mirror plane perpendicular to b.

For H along the b axis, on the other hand, it is possible to have the applied field add to the exchange field of one site and subtract from that of the other, giving a double optical line pattern which is very difficult to interpret. According to the model, the energy-level splittings in either the upper or lower state of a transition for H along the b axis would be given by the nonlinear expressions for $W(1b)$ and $W(2b)$ given as the third entry in Table II.

The g factors and effective field for the upper and lower states of a given optical transition are, in general, different, and it is not necessary that the x and y axes have the same direction for every level.[19] We assume, however, that H_{eff} is the same for all levels derived from a single spin-orbit manifold and initially that the site axes are the same for all states. There are, then, ten constants in general involved in every set of optical lines for $H\|b$, and the assumption of equal ϑ, φ, and H_{eff} for all lines in a manifold reduces it to seven. We have attempted to derive these seven constants from the line patterns in the following way: Since the identity of each line in a pattern is not clearly assignable in the beginning to a particular transition, and since many qualitatively different nonlinear Zeeman patterns may be obtained with different combinations of upper- and lower-state g factors, we have computed what the expected patterns should look like for various values of the seven constants and compared them qualitatively with the patterns we have observed. Recognition of a qualitative pattern then allows identification of the individual transitions, and the appropriate energy differences

TABLE III. Values of constants used in formulas of Table II to match the observed $ErFeO_3$ Zeeman pattern.

$E=0$ ground level	$E=45.7$-cm^{-1} state
$H_{\text{eff}}=12\,000$ Oe	$H_{\text{eff}}=12\,000$ Oe
$\vartheta=41°$	$\vartheta=31°$
$\varphi=40°$	$\varphi=50°$
$(\vartheta+\varphi)=81°$	$(\vartheta+\varphi)=81°$
$g_x=1.2$	$g_x=4.1$
$g_y=4.5$	$g_y=0.7$
$g_z=5.76$	$g_z=1.78$

[19] H. Lämmermann, Z. Physik **150**, 551 (1958).

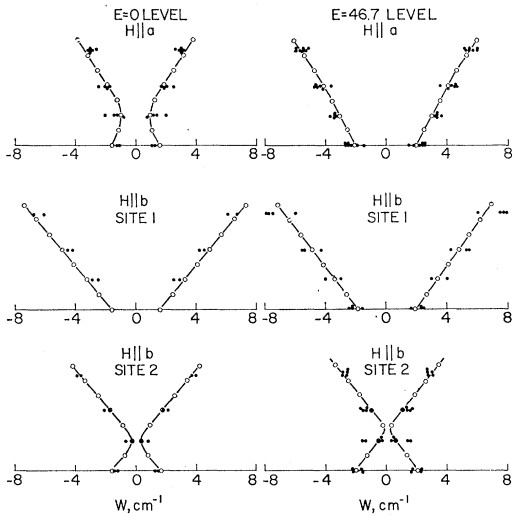

FIG. 6. Nonlinear Zeeman splitting of ground state (left) and first excited state (right) of Er^{3+} in $ErFeO_3$ at 77°K for magnetic fields applied parallel to the crystal a, b, and c axes. Open circles and curves are computed splittings using parameters from Table III. Filled circles are experimental points obtained by analysis of Zeeman line patterns as described in the text.

give the level splittings for the upper and lower states. The computed patterns were generated by a digital computer which plotted the patterns on a photographic output device, and all experimental observations were reduced to energy-level positions from the line identification through the comparison of experimental and computed patterns before attempting to derive the constants required by the model. We found initially a single set of constants which simultaneously gave a rough fit to the energy-level data for the two lowest Er^{3+} levels for applied fields parallel to the a and b axes. It was impossible, however, to refine the fit without allowing for different site-axis orientations for the two states. Note that the direction of H_{eff} is given by ϑ and φ in Table III (Fig. 1) because of our choice of variables, and variation of φ in fitting the experimental data required a compensating variation in ϑ to keep $\vartheta+\varphi$ constant. With the freedom to choose different site-axis directions for different energy levels, it was possible to refine the fit to that shown in Fig. 6 using the constants listed in Table III. The calculated points are the open circles in the figure, and the filled circles are experimental points representing 27 lines for which the patterns could be analyzed. It can be seen that the assumption of a constant effective field and differing site axes for the two levels gives a good fit to the optical data.

SUBLATTICE MAGNETIZATIONS AND EXCHANGE FIELDS

Sublattice magnetizations for Er^{3+} have been calculated from standard formulas[20] using the parameters in

[20] J. H. Van Vleck, *Theory of Electric and Magnetic Susceptibilities* (Oxford University Press, London, 1932).

TABLE IV. Magnetic dipolar fields[a] in $ErFeO_3$.

Position of Er^{3+} ion	$T>T_r$ (Oe) H_a	H_b	H_c	$T<T_r$ (Oe) H_a	H_b	H_c
$(\frac{1}{2}a-x, \frac{1}{2}b+y, \frac{1}{4}c)$	0	0	925	925	−3076	0
$(x,y,\frac{1}{4}c)$	0	0	925	925	3076	0

[a] Algebraic signs would all reverse on reversing the Fe^{3+} spins (see text).

Table III. The calculated magnetization vectors increase in magnitude and swing away from the b axis as the temperature decreases (Fig. 7). If the Fe^{3+} spins contribute a constant magnetization, $\sigma(\mathrm{Fe})\approx 1.4$ emu/g as observed[21] in $YFeO_3$, then the net magnetization should drop to zero at about $T_0\approx 50°K$. It is gratifying to note that a compensation point is observed[15] in $ErFeO_3$ at $T_0\approx 45°K$, in reasonable agreement with the predicted value. Precise agreement between calculated and observed magnetizations is not expected for the following reasons: (a) The Fe^{3+} contributions are not known precisely; (b) the g factors (Table III) are, at best, accurate to two places; and (c) energy shifts (~ 0.1 cm^{-1}) which are second order in H_{eff} can seriously influence the magnetization at higher temperatures,[22] but could not be measured spectroscopically. We feel that having obtained qualitatively the correct temperature dependence for the magnetization gives additional justification for the various assumptions made in reducing the complicated Zeeman pattern.

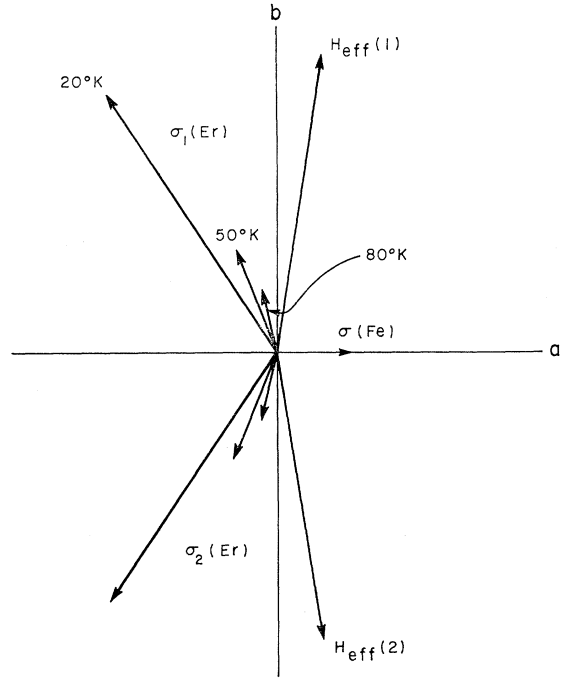

FIG. 7. Effective fields H_{eff} and calculated rare-earth sublattice magnetizations $\sigma(Er)$ at three temperatures in $ErFeO_3$. The magnetization vectors are drawn to scale. The iron sublattice magnetization is assumed to be $\sigma(\mathrm{Fe})\approx 1.4$ emu/g (see text).

The values we have obtained for H_{eff} include both magnetic dipolar and exchange contributions. The portion of the Hamiltonian for the Er^{3+} ions which describes the interactions with the Fe^{3+} ions may be written[23]

$$-g_J\beta\mathbf{J}\cdot\mathbf{H}_{\mathrm{eff}}=-g_J\beta\mathbf{J}\cdot\{\mathbf{H}_{\mathrm{dip}}+2[(g_J-1)/g_J]\mathbf{H}_{\mathrm{ex}}\},$$

where g_J is the Landé g factor. The exchange field $\mathbf{H}_{\mathrm{ex}}$ acts only on the spin of the Er^{3+} ion, as given by the factor (g_J-1) times the total angular momentum J. Substituting $g_J=6/5$ for the $^4I_{15/2}$ manifold of Er^{3+} into the expression above, we find

$$\mathbf{H}_{\mathrm{ex}}=3(\mathbf{H}_{\mathrm{eff}}-\mathbf{H}_{\mathrm{dip}}).$$

The dipolar fields in $ErFeO_3$ have been calculated (Table IV) using Bertaut's technique[14] and the crystallographic parameters summarized by Faulhaber *et al.*[5] The magnetic moment was assumed to be 5β for the Fe^{3+} ions and the small canting angle[12] (8 mrad) was neglected. We assigned the signature $+1$ to the Fe^{3+} spins at $(\frac{1}{2},0,0)$ and $(0,\frac{1}{2},\frac{1}{2})$ in the unit cell, and -1 to those at $(\frac{1}{2},0,\frac{1}{2})$ and $(0,\frac{1}{2},0)$. For a real crystal of $ErFeO_3$ at, e.g., room temperature, the direction of net magnetization would change from $+c$ to $-c$ on reversing all of the Fe^{3+} spins. This would also reverse the sign on the dipolar fields at the Er^{3+} sites. We do not know which choice of signs for the Fe^{3+} spins corresponds to a magnetization along $+c$ at room temperature (or along $+a$ for $T<T_r$). This is because the canting angle was too small to be detected in the neutron-diffraction study[11] of $ErFeO_3$. Thus, all of the components listed in Table IV must be regarded as uncertain to a factor ± 1. In comparing with our optical data, a further uncertainty arises, since we cannot know which of the two crystallographic sites corresponds to our "site 1."

From the experimentally determined value for $\mathbf{H}_{\mathrm{eff}}$ and the (fourfold uncertain) results for $\mathbf{H}_{\mathrm{dip}}$ we obtain values for $\mathbf{H}_{\mathrm{ex}}$, as listed in Table V. Summarizing from the Table, $\mathbf{H}_{\mathrm{ex}}$ is in the a-b plane, has a magnitude of either about 27 kOe or about 45 kOe, and lies not far ($\lesssim 18°$) from the b axis of the crystal.

DISCUSSION

The value we obtain for H_{eff} may be compared with that obtained in other studies of rare-earth–iron coupling in the orthoferrites, $RFeO_3$. At high temperatures ($T>T_r$), H_{eff} lies along the c axis. An indication of its size was obtained[12] by comparing measured[24] bulk magnetization and Fe^{3+} magnetization (as measured[13]

[21] V. M. Jidin, A. B. Sherman, and J. E. Myl'nikova, Phys. Letters **22**, 554 (1966).

[22] The necessity of including second-order contributions has been emphasized in Ref. 8, where the Fe^{3+}-Er^{3+} coupling energy for $T<T_r$ was estimated from the spectroscopic data.

[23] W. P. Wolf and J. H. Van Vleck, Phys. Rev. **118**, 1490 (1960).

[24] G. Gorodetsky and D. Treves, in *Proceedings of the International Conference on Magnetism, Nottingham, 1964* (The Institute of Physics and The Physical Society, London, 1965), p. 606.

by the Mössbauer effect). It was assumed that the canting angle for the Fe^{3+} sublattices remained independent of temperature and that the R^{3+} contributions could be written $\chi(R^{3+})\,H_{\rm eff}$, where $H_{\rm eff}$ is proportional to the Fe^{3+} magnetization, and $\chi(R^{3+})$ follows Curie's law $C(R^{3+})/T$. To obtain numerical values for $H_{\rm eff}$, the Curie constants, $C(R^{3+})$, were set equal to the values for free ions. This last approximation is accurate only at very high temperatures in these materials, but the procedure can be expected to give the correct order of magnitude for $H_{\rm eff}$. The derived values[12] ranged from 0.9 kOe, for R=Ho, to 7.6 kOe, for R=*Nd*. For $ErFeO_3$, the value $H_{\rm eff}=-1$ kOe was obtained. This is an order of magnitude smaller than our value of 12 kOe at $T<T_r$, which is consistent with our observation[8] that the Er^{3+} splittings decrease by at least a factor of 4 on traversing the reorientation region. It may be seen from Table IV that magnetic dipolar fields make up a significant fraction of $H_{\rm eff}$ for $T>T_r$.

Optical spectroscopy[5] and the Mössbauer effect[25] have been used to study interactions in $ErFeO_3$ at pumped liquid-helium temperatures, where the Er^{3+} sublattices become magnetically ordered[11] along the c axis of the crystal. Both techniques gave a splitting for the ground state of about 6.2 cm^{-1} and a magnetic moment of 6.6β at the lowest temperatures, yielding a total effective field of about 10 kOe. In this case the effective field includes both Er^{3+}-Er^{3+} and Er^{3+}-Fe^{3+} interaction. The effective field is about the same as we measure at higher temperatures, but the splitting of the ground state is greater (and, therefore, the interaction energy is more negative), because of the larger g factor for fields along the c axis of the crystal.

Our derived value for the exchange field (27 or 45 kOe) at $T<T_r$ may be compared with the exchange field $\sim$300 kOe, which describes the polarization of the R^{3+} ions by the Fe^{3+} spins in the garnets $R_3Fe_5O_{12}$.[23,26] These compounds are ferrimagnetic, with the Fe^{3+} ions contributing 5β per formula unit, as compared to about 0.05β obtained from the canting of the Fe^{3+} sublattices in the orthoferrites. An appreciable fraction of the symmetric exchange in the orthoferrites is certainly cancelled out by the (nearly) antiparallel arrangement of Fe^{3+} spins on the interpenetrating sublattices[11] surrounding the R^{3+} ions. This, apart from other geometrical factors, could explain a tenfold difference in exchange interactions between the two series of compounds.

The exchange fields in $ErFeO_3$ have been shown to lie close to the $\pm b$ axes at the two Er^{3+} sites for $T<T_r$. The Fe^{3+} spins lie nearly along the $\pm c$ axes, while the net magnetization arising from canting of the Fe^{3+} spins is along the a axis. In a rigorous, four-sublattice model[14,15] for the Fe^{3+} sublattices, the Fe^{3+} spins also may have components (summing to zero) along the $\pm b$ axes. Our experimentally determined exchange field, therefore, may arise from (a) antisymmetric coupling[27] to the c components of the Fe^{3+} spins, (b) antisymmetric coupling to the a components of the Fe^{3+} spins, or (c) symmetric coupling to the b components of the Fe^{3+} spins. It is not possible to decide among the three possibilities at this point. However, we may conclude that (a) this is a situation in which the simple two-sublattice model for the Fe^{3+} spins is not applicable, and/or (b) we have significant antisymmetric coupling between Er^{3+} and Fe^{3+} ions in this structure.

TABLE V. Components of internal fields, evaluated for $T<T_r$ at "site 1" in $ErFeO_3$.

$H_{\rm eff}$ (kOe)[a]		$H_{\rm dip}$ (kOe)[b,c]		$H_{\rm ex}$ (kOe)[c]	
a axis	b axis	a axis	b axis	a axis	b axis
1.88	11.85	0.925	−3.08	2.86	44.8
1.88	11.85	0.925	3.08	2.86	26.3
1.88	11.85	−0.925	3.08	8.41	26.3
1.88	11.85	−0.925	−3.08	8.41	44.8

[a] From Table III.
[b] From Table IV.
[c] We list four possible sets of values because we do not know the algebraic sign on the Fe^{3+} spins or which of the two crystallographic sites (Table IV) corresponds to our "site 1."

CONCLUSION

This study has provided new information on the magnetic behavior and exchange interactions in $ErFeO_3$. It has been possible to understand the very complicated Zeeman patterns in terms of a simple model involving two inequivalent sites for the Er^{3+} ions. The interactions with the Fe^{3+} ions could be described with molecular fields. The results of analyzing the Zeeman patterns were shown to be consistent, in general terms, with the bulk magnetic properties of $ErFeO_3$. It was especially helpful to be able to study both the crystal field ground state for Er^{3+} and the first excited doublet, as both levels are populated at temperatures $\gtrsim$50°K. Using optical spectroscopy, a detailed picture was obtained of the magnetic behavior for $T<T_r$ in $ErFeO_3$.

ACKNOWLEDGMENTS

We are indebted to W. E. Burke and E. M. Kelly for experimental assistance, and to E. M. Gyorgy and S. Hüfner for helpful discussions.

[25] W. Wiedemann and W. Zinn, Z. Angew. Phys. **20**, 327 (1966); I. Nowik and H. H. Wickman, Phys. Rev. Letters **17**, 949 (1966).
[26] R. Pauthenet, Ann. Phys. (Paris) **3**, 424 (1958).
[27] P. M. Levy [Phys. Rev. Letters **20**, 1366 (1968)] has demonstrated theoretically the possibility of significant antisymmetric contributions to the exchange tensor for rare-earth ions.